Thermal analysis of eutectic alloy at HBC fuses

L.-G. BUJOREANU[a], N. M. LOHAN[a], M.-G. SURU[a], A. PLESCA[b*]
[a]*Faculty of Materials Science and Engineering, The "Gheorghe Asachi" Technical University of Iaşi, Bd. D. Mangeron 67, 700050 Iaşi, Romania*
[b]*Faculty of Electrical Engineering, Energetics and Applied Informatics, The "Gheorghe Asachi" Technical University of Iaşi, Bd. D. Mangeron 21-23, 700050 Iaşi, Romania*

Fuses are one of the most used electrical apparatus to protect different type of electrical installations against overloads and short circuits. In this paper, the metallurgical (M)-effect under different overloads has been experimentally established, by analyzing the evolution of executive eutectic element at different heating rates. Two mathematical functions were derived aiming to approximate the dissolution depth variation against time and temperatures, during the service of a high breaking capacity (HBC) device. One of the equations, of exponential type, can be used with good accuracy in the range of low temperatures while the other one, a compact equation, is more suitable for high heating temperatures of the eutectic alloy, actually corresponding to high overloads. The comparison between experimental and analytical results validates the applicability of the proposed mathematical models of the dissolution depth. The eutectic alloy was investigated by differential scanning calorimetry (DSC) and optical microscopy (OM) and a correlation between heating rate, melting temperatures and eutectic morphology was discussed.

(Received April 9, 2015; accepted September 9, 2015)

Keywords: mathematical model, eutectic alloy, HBC fuse, DSC thermogram, OM microstructure

1. Introduction

There are many types of fuses used to protect different electrical apparatus, circuits and equipment. High breaking capacity (HBC) fuse-links have been used for more than a century in many protection devices owing to the fast interrupting of the highest fault currents and to their simplicity. HBC fuses are generally composed of a single thin fuse-element strip or a number of parallel connected fuse-elements, usually in copper, with one or more shares of reduced cross section areas called notches [1]. These setups are designed having different shapes such as circular, rectangular or trapezoidal, and thus the thermal analysis could be considered as for a variable cross-section fuse links, through which passes the necessary current [2]. The conductor element is usually surrounded by silica sand and enclosed in a robust mechanical ceramic body. Due to the fuse-element complex geometry and the filling material heterogeneities, HBC fuses have a rather complex behaviour. HBC fuses generally operate in two characteristic time ranges that involve different physical processes, namely, pre-arcing and arcing times [3]. A two-dimensional mathematical model was developed by [3] in order to study the short pre-arcing period in HBC fuses. This model has been useful in obtaining the inverse pre-arcing time/current characteristics for industrial fuse-elements of various geometries. There are many tests with different materials used for HBC fuse fillers, such as aluminium hydro-oxide, boric acid, zinc oxide, titanium oxide, and boron trioxide and their results are compared with those on silica sand at high currents. The study demonstrates that silica sand is superior filler in HBC fuses for heavy current interruption as compared to other tested compounds [4]. Different tests were made on HBC fuses as in [5, 6] where the closing angle and the power factor, were used to characterize electrical fault test conditions close to the industrial test conditions and required by international standards. A resistive power factor gives fault current higher than the inductive power factor, and then the pre-arcing time was found to be longer in the inductive case as compared to the pre-arcing time in the resistive case. The role played by the closing angle in the pre-arcing duration was analysed and it was found that typical closing angle values involve maximum dissipated energy which is interesting for Joule integral prediction. In order to analyse the heat flow and diffusion effects which simultaneously occur during the pre-0arcing period of a fuse with metallurgical (M)-effect, a method has been developed to model the fuse operation as an electrical circuit. The method enabled for plane elements, notched elements and elements both with and without M-effect to be modelled. The portion of the fuse element containing the M-effect alloy was considered to consist of a large number of small cells each possessing uniform properties at any given instant of time. These properties include temperature, electrical resistivity, thermal conductivity and diffusion coefficient. For fuses with M-effect, when temperature and diffusion are actively involved, good agreement is obtained for operating times up to approximately 30 min [7]. Analysis of M-effect operation not only requires the current distribution and the temperature rise to be determined, but also the rate of diffusion of the M-effect alloy through the fuse element. In the M-effect region the current will vary in three dimensions and the calculation of current flow involves the solution of Laplace's equation for a three-dimensional

system of non-uniform conductivity [8]. In [9], a Windows based program code was developed for modelling complete fuses, including M-Effect, by using the Finite Volume Method (FEM) [9]. Another model for HBC fuse-link was developed based on time-current characteristic fuse and implemented in Matlab [10]. The simulation results, for normal operation using the developed model of the HBC fuse-link has demonstrated that a problem might occur when using an unsuitable HBC fuse-links (occurrence of nuisance operation). Fuse thermal analysis has been modelled and simulated also in ANSYS, as in [11]. The fuses have been simulated under sinusoidal current and different parameters such as temperature distribution, thermal flux, voltage, and so on, relating to various parts of fuse have been obtained and investigated.

In recent years, a new generation of solders has been developed in order to replace Pb-Sn solders with lead-free solder alloys. Many of the proposed alloy systems are Sn-rich alloys [12]. In [12] a SnCu1 lead-free solder is analysed. The major factors affecting a solder selection are the melting point of an alloy, the wetting characteristics, the cost, the availability, the environment. The results showed that the dissolution of the copper wire during hot dipping at a selected working temperature can be attributed to the increased solubility of the copper in the liquid solder and a prolonged time of dipping. The Sn-Zn alloy has been investigated [13] as an alternative Pb-free alloy for low-voltage fuse elements. The temperature dependence of specific resistivity and thermal conductivity for some Sn-Zn alloys was measured in order to use their values in electrical and thermal calculations on the basis of Ohm's and Fourier's laws, aiming to obtain the temperature-distribution in lead-free fuse elements of electric power line. Specific resistivity and thermal conductivity could be estimated as a function of temperature and alloy composition in the compositional ranges classified from the point of view of continuity or non-continuity of constituent phases such as primary Zn, Sn-solid solution and eutectic in microstructures of Sn-1 to 100Zn alloys [13]. For the Pb-free fuse elements, used in electric power line, the addition of 8 vol. % Al_2O_3 in Zn-50 mass %Sn was carried out for the control of electrical and thermal properties. Homogeneous and heterogeneous Al_2O_3-distributions were achieved in microstructure consisting of primary Zn and eutectic. Both the melt and un-melt performance for AC-low voltage fuse elements could be satisfied on both Zn-50Sn alloys with different distribution of Al_2O_3, and the superior performance was shown in the homogeneously Al_2O_3 distributed alloy [14]. Among several candidate alloys, the Sn–Ag–Cu alloy family is believed to be the first choice with the combination of other alloys such as Sn–Zn–Bi, Sn–Cu and Sn–Bi–Ag. The Cu6Sn5/Cu3Sn layers are formed at most lead-free solder alloy/Cu interfaces, while Cu–Zn compound layers are formed in the Sn–Zn/Cu system. Others tests were made with alternative alloys Sn-Bi, Sn-In and ternary alloys Sn-Bi-Cu and Sn-In-Cu [15]. The ternary system Sn-Bi-Cu was found to give best results and showed the same time-temperature-dissolution-behaviour during the M-effect as the SnCd20 solder. The low melting alloy of tin, bismuth and antimony named alloy ETI-Sn-Bi-Sb is ecologically safe, and by its technical and physical properties (melting point, conductivity, wettability) corresponds to the requirements of the use for fusible elements of low voltage fuses [16].

2. Mathematical model

The analyzed fuse was a gG type, size 2, with rated current by 160A, rated voltage about 550V, rated power losses of 12.8W and rated breaking capacity of 120kA. The fuse has the following overall dimensions: length of the ceramic body: 61mm, square cross-section: 50mm × 50mm, total length including the knife contacts: 150mm, total length of the fuse-holder: 230mm. The fuse link has a length of 55mm, width about 10mm and thickness of 0.2mm. The fuse consists of a steatite made ceramic body, copper knives, aluminium lids, copper fuse links 99.9% and quartz sand as filler material of grains among sieves 30 and 50. The low melting temperature, actually the M-effect, is based on Pb-Sn eutectic alloy. When the M-effect reaches the melting temperature, it dissolves the base material (fuse element) in such a way as to form a compound with higher resistivity, having an initiator effect, unchaining an accumulative process that erodes the metal bases (copper) increasing its resistance and generates heat till the total melting of the metal bases and the electric arc will start. In the case when the amount of the released energy is not enough to liquefy the eutectic alloy, the breakup process of the fuse link doesn't take place. If there are load picks or high recurrent overloads, it is possible to start the breakup process even in advance, till the fuse link is melted even in the case of smaller currents than its rated value.

Nowadays, the operation of the HBC fuse can be established by means of analytical models of high complexity which allow the researcher to achieve extremely reasonable approaches. More accurate results can be obtained using modelling and simulation commercial software based on finite elements, for instance. The modelling of the diffusion process allow to verify the protection against overload of power electrical equipment, in general, and of the cables, in particular, especially in those cases where the electric circuit is subjected to recurrent overloads.

The diffusion process has been investigated at different overload currents (250, 270, 300, 400 and 500A). Using proper type K thermocouples, the temperatures of the eutectic alloy on the fuse link have been measured (acquired). The small voltage signals provided by thermocouples have been amplified using a signal conditioning board type AT2F-16 with the error of ± 0.5%. The amplified signal was the input for a data acquisition board type PC-LPM-16 which can be programmed with LabVIEW software. The sampling rate was 50kS/s and the analogue inputs have a resolution on 12 bits. After the fuse interruption, the fuse links with the eutectic alloy were removed from the fuse body. The alloy samples have been embedded into mounting resin. The test

samples were ground, till reaching the mirrored surface, by means of the abrasive paper with mesh no. from 200 up to 800, final polishing being made a finished with alumina suspension. Then, the diffusion depth has been measured using a metallographic microscope with a magnification of 200x. The penetration depth in function of time, for different temperatures, is shown in Fig. 1.

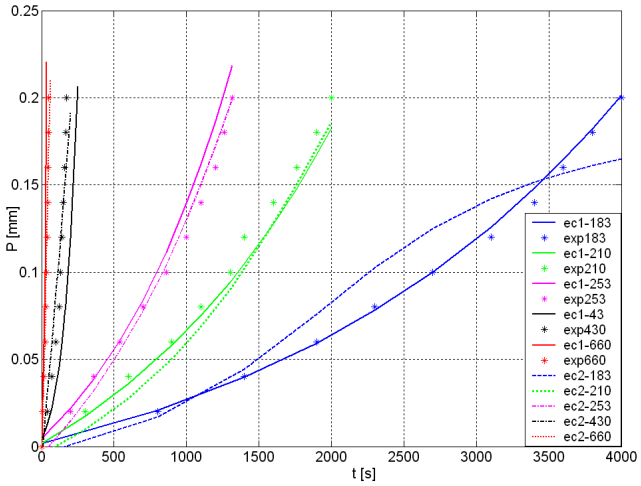

Fig. 1. The variation of penetration depth with time at different temperatures (183, 210, 253, 430 and 660ºC). Comparison between experimental values (exp183, exp210, exp253, exp430, exp660), first equation of approximation (ec1-183, ec1-210, ec1-253, ec1-430, ec1-660) and second equation of approximation (ec2-183, ec2-210, ec2-253, ec2-430, ec2-660)

Using specific software, a mathematical model was obtained for the penetration depth as a function of time and temperature. There are two solutions:

2.1. An exponential function

The penetration depth can be determined with the following exponential function,

$$P(\theta,t) = a(\theta) + b(\theta)\cdot e^{-\frac{t}{c(\theta)}} \qquad (1)$$

where:

$a(\theta) = a' + \frac{b'}{\ln\theta} + \frac{\ln\theta}{\theta^{c'}} + \frac{d'}{\theta^{2}}$, with the coefficients:

a = -3.08295; b = 21.46858; c = -59366.157;
d = 272852.1333

$b(\theta) = a'' + b''\ln\theta + \frac{c''}{\theta} + \frac{d''}{\theta^{0.5}}$, with the coefficients:

$a' = 1.19684$; $b' = -1247.9552$; $c' = 8502.9407$;
$d' = -29915.8642$

$c(\theta) = a'' + b''\ln\theta + \frac{c''}{\ln\theta} + \frac{d''}{\theta^{1.5}}$, with the coefficients:

$a'' = 7109905.0547$; $b'' = -357900.6255$;
$c'' = -38203934.345$; $d'' = 28213436.40038$

2.2. A compact function

This solution is based on a non-linear lorentzian cumulative function,

$$P(\theta,t) = a + b\left[\frac{1}{2} + \frac{arctg\left(\frac{t-c}{d}\right)}{\pi}\right] + e\left[\frac{1}{2} + \frac{arctg\left(\frac{\theta-f}{g}\right)}{\pi}\right] + h\left[\frac{1}{2} + \frac{arctg\left(\frac{t-c}{d}\right)}{\pi}\right]\left[\frac{1}{2} + \frac{arctg\left(\frac{\theta-f}{g}\right)}{\pi}\right] \qquad (2)$$

where the coefficients are: a = 0.5; b = -2.8291;
c = 1951.598; d = 1220.639; e = -10.3309; f = 474.8228;
g = 49.29626; h = 57.98634

The advantage of the second solution is represented by the compact form of the mathematical function and the smaller number of the coefficients as compared to the first one. Also, the coefficient values of the compact function are more reasonable from computing point of view, than those of the exponential function.

The comparison between the experimental values and those determined with both proposed mathematical models, for the penetration depth of the eutectic alloy, is presented in the same Fig. 1. The curves variation covers a penetration range up to around 0.2mm of dissolution depth which means actually the thickness of the copper fuse link. When the penetration depth reaches the value of 0.2mm, it means the fuse link is broken and the fuse operates by interrupting the main electrical circuit to be protected against fault currents. From the diagrams, it can be noticed that at higher temperatures, θ = 660ºC (exp660), the time when the penetration depth reaches the critical value of 0.2mm, is decreased (around 50 seconds), with respect to the lower temperatures, θ = 183ºC (exp183) when the operation time is about 4000 seconds, Fig. 1. With the aim to increase the clarity of the variation curves especially at high temperatures, when the operating times are low, the diagrams have been represented in logarithmic time axis, Fig. 2. It can be observed that the first equation, the exponential function, approximates, in a higher degree, the evolution of the penetration depth in the range of low temperatures from θ = 183ºC (ec1-183) to θ = 253ºC (ec1-253), Fig. 1, and the second function, the compact equation, is more suitable to be used at high temperatures, from θ = 253ºC (ec2-253) to θ = 660ºC (ec2-660), Fig. 2.

The above proposed mathematical functions enable to compute the dissolution depth of the fuse link at certain temperatures, actually, at certain overloads.

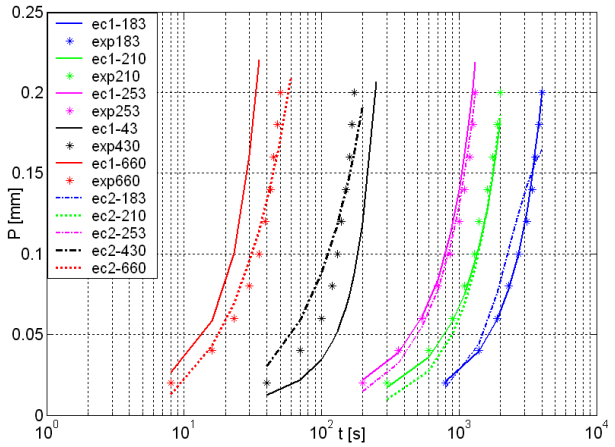

Fig. 2. The penetration depth variation with logarithmic time axis at different temperatures (183, 210, 253, 430 and 660ºC). Comparison between experimental values (exp183, exp210, exp253, exp430, exp660), first equation of approximation (ec1-183, ec1-210, ec1-253, ec1-430, ec1-660) and second equation of approximation (ec2-183, ec2-210, ec2-253, ec2-430, ec2-660)

Hence, there is the possibility to calculate the operating time of the fuse under different overloads, actually the protection characteristic of the HBC fuse which uses this type of eutectic alloy (Pb-Sn) for M-effect. Therefore, the composition of the eutectic alloy may influence the protection characteristic of the HBC fuse.

Different values of electric overloads mean different heating rates for the eutectic alloy. Using Pro/Mechanica specific software, based on finite element method, the correlation between the values of the overloads and the heating rate has been established, according to Table 1. This correlation can be used to make the eutectic alloy analysis from material structure point of view, as presented in the next section.

Table 1: Correlation between the values of the overloads and the heating rate

Overload [A]	250	270	300	400
Heating rate [K/min]	5	10	20	40

3. Eutectic material analysis

Several fuses were burned on purpose, in an experimental set-up, with the same rated current of 160 A. After circuit breaking, the fuses were dismantled and the eutectic alloy was removed from the fuse link. Four eutectic fragments, weighing up to 50 mg, which underwent a melting-solidification process, were further subjected to differential scanning calorimetry (DSC) analyses, by means of a Netzsch calorimeter type DSC 200 F3 Maia. The device was calibrated with Bi, In, Sn and Zn standards. The measurements were performed by heating under Ar protective atmosphere using corresponding correction curves, for each thermal series. The four fragments were heated with: (i) 5K/min; (ii) 10K/min; (iii) 20K/min and 40K/min, up to 300^{0}C.

After DSC scans, the eutectic fragments underwent second melting-solidification cycle. The fragments were removed from DSC crucible and embedded into Mécaprex KM-U cold mounting resin, before being metallographically prepared by grinding, polishing and etching. Optical microscopy (OM) observations were performed on an OPTIKA XDS-3 MET microscope equipped with OPTIKAM 4083.B5 microscopy digital USB camera and OPTIKAM B5 software.

4. Experimental results and discussions

The first DSC chart presents in Fig. 3, the melting behaviour of the eutectic alloy fragment heated with 5K/ min. Melting started at 185^{0}C and ended at 191.7^{0}C, reaching a maximum transformation rate at 190.6^{0}C. The heat flow value corresponding to DSC peak was 0.579 mW/ mg. Absorbed heat was 26.91 J/g.

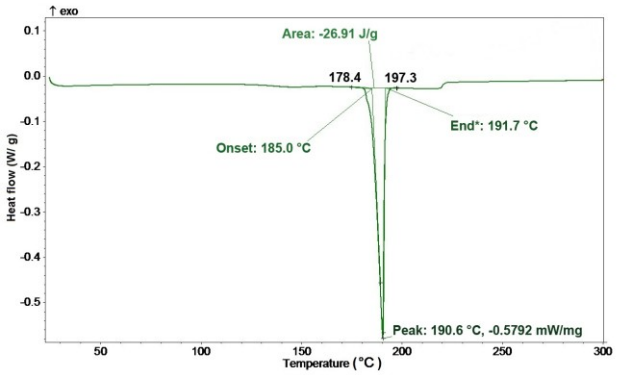

Fig. 3. Typical DSC thermogram recorded during specimen heating at 5 K/ min

The increase of heating rate, to 10 K/min caused a change of DSC chart, according to Fig. 4. Melting occurred between 184.9^{0}C and 192.7^{0}C, with maximum transformation rate at the same temperature of 190.6^{0}C.

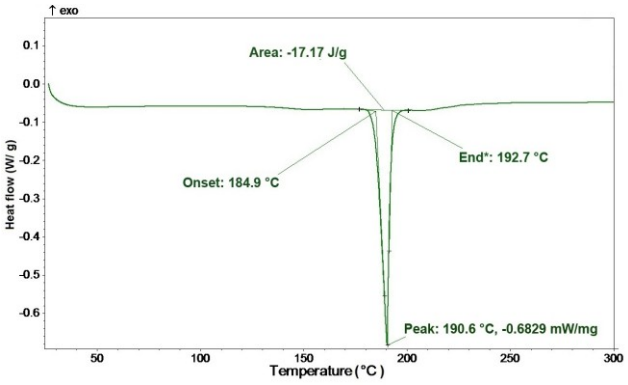

Fig. 4. Typical DSC thermogram recorded during specimen heating at 10 K/ min

The heat flow value corresponding to DSC peak increased to 0.683 mW/ mg. In this case, absorbed heat decreased to 17.17 J/g. Nevertheless, it may be assumed that the increase of heating rate from 5 to 10K/min caused

only minor changes of the melting behaviour of eutectic alloy.

The third heating rate, 20K/min caused noticeable changes in the position and shape of corresponding DSC chart, as shown in Fig. 5. Melting started at 188^{0}C, reached maximum transformation rate at 205.1^{0}C, at a corresponding heat flow value of 1.204 mW/ mg and ended at 212.2^{0}C. In addition, absorbed melting heat increased to 43.53 J/ g. Thus the increase of heating rate, from 5 to 20K/min (4 times) caused increases of conventional transformation interval (difference between end and onset temperatures) from almost 7^{0}C to more than 24^{0}C (3.4 times) and of maximum absolute value of heat flow from 0.579 to 1.204 mW/mg (more than 2 times).

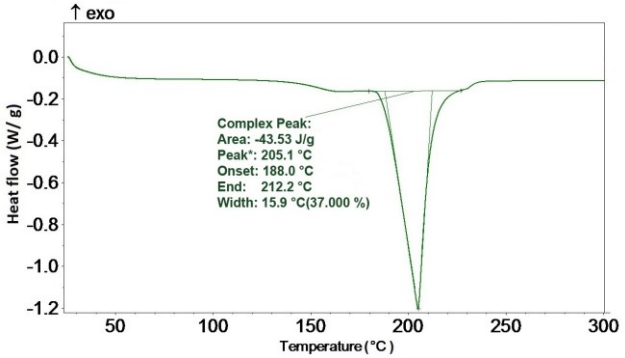

Fig. 5. Typical DSC thermogram recorded during specimen heating at 20 K/ min

The last heating rate was 40 K/min. In this case, shown in Fig. 6, a heating-cooling-heating sequence was chosen, in order to emphasize heating rate effects. The eutectic alloy fragment, heated with this rate, melt between 189 and 211^{0}C in the first cycle and between 186.9 and 204.7^{0}C, in the second.

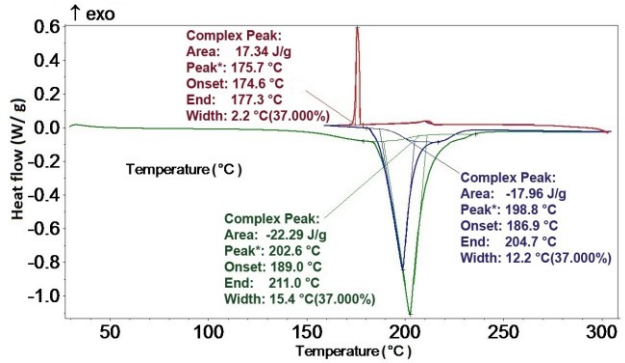

Fig. 6. Typical DSC thermogram recorded during specimen heating at 40 K/ min

It is noticeable that, between the two melting stages, solidification occurred being accompanied by an exothermic peak, located at 175.7^{0}C and a released specific heat of 17.34 J/g. Since the value of absorbed specific heat in the second melting cycle is 17.96 J/g, it follows that the two phenomena are thermally reversible.

When summarizing DSC data, the influence of heating rate on critical temperatures can be observed. Thus, Fig. 7 shows that the increase of heating rate, which has a marked effect on the critical temperatures of solid state transitions [17], caused a general increasing tendency of onset, peak and end temperatures of melting.

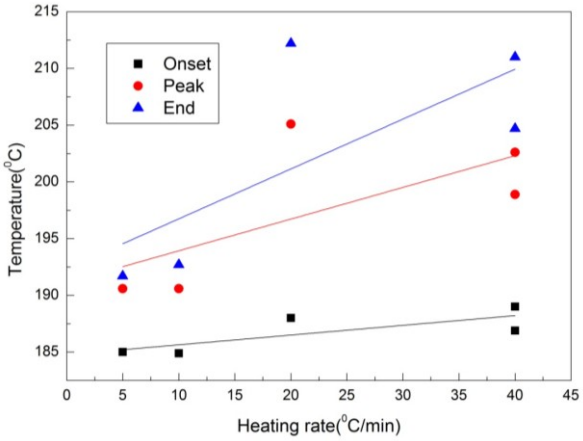

Fig. 7. Summary of DSC critical temperatures associated with melting and variation tendencies with heating rate

After the DSC scans, the respective specimens were removed from calorimeter crucible and prepared for optical microscopy (OM) observations. The first micrographs are illustrated in Fig. 8, corresponding to the specimen scanned with 5K/ min.

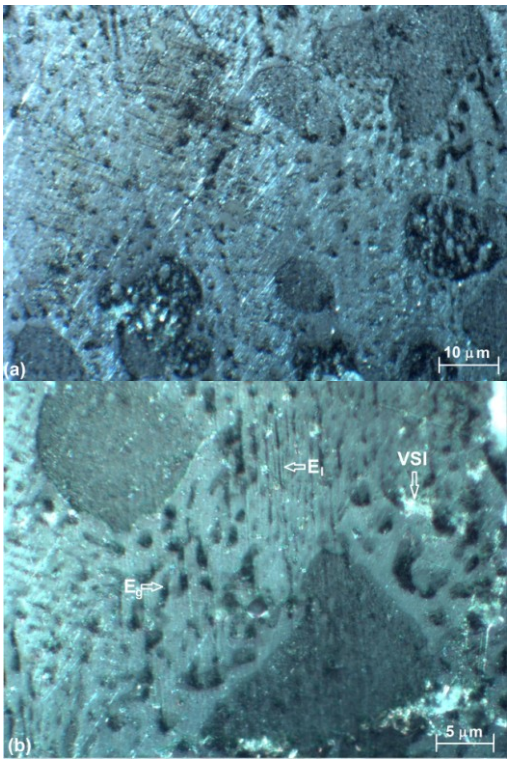

Fig. 8. OM micrographs of the specimen heated with 5K/min: (a) general aspect; (b) detail of the areas with lamellar eutectic (E_l), globular eutectic (E_g) and vitrified sand islands (VSI)

Fig. 8(a) presents the general aspect of the structure which is typical for Pb-Sn hypoeutectic solders. Pb-Sn eutectic contains 61.9 %Sn and presents lamellar structure, after low solidification rates, which becomes globular at high rates, [18]. In Fig. 8(a) the structure contains a mixture of lamellar and globular eutectic. Since the increase of heating rate was accompanied by an augmentation tendency of all critical temperatures associated with melting, it can be assumed that heating rate increase amplified melt overheating. Considering overheated liquid solders, subjected to free-air cooling, it can be assumed that with the increase of heating rate, the melt will be heated to a more elevated temperature. Since the melt is subjected to free-air cooling, the difference between overheated (melt) solder and room temperature will increase with increasing the heating rate. During air-cooling, solidification occurs and its rate increases with the temperature of previous overheating. In other words, it can be assumed that the larger the heating rate (causing melting) the larger the solidification rate, during subsequent cooling. Under these circumstances it can be assumed that a heating rate of 5K/min can be associated with an intermediary subsequent solidification rate of liquid melt.

The detail of Fig.8(b) reveals the characteristics of eutectic matrix which, besides globular eutectic (E_g) and lamellar eutectic (E_l), also contains some isolated vitrified sand islands (VSI). In addition, to eutectic matrix, the micrograph contains dark dendritic grains of Pb-rich pro-eutectic solid solution. The general aspect of the microstructure corresponds to the typical characteristic of Pb-50 mass. % Sn solders [18].

The increase of solidification rate, after the melting caused by a heating rate of to 10K/min, was accompanied by the augmentation of globular eutectic (E_g), as shown in Fig. 9(a). The detail from Fig. 9(b) shows that most of Pb-rich solid solution, from eutectic constitution, has globular form.

Further increasing solidification rate due to melting with a heating rate of 20K/min caused the disappearance of almost all lamellar eutectic, according to Fig. 10(a). However, at larger magnification, some isolated lamellar areas can be observed, as exemplified by white arrows in Fig. 10(b).

Finally, after the solidification process subsequent the melting caused by a heating rate of 40K/min, lamellar eutectic structures are no longer noticeable, as shown in Fig. 11(a). Due to large heating rate, large areas of vitrified sand (VS) are noticed Fig. 11(b). All these microstructural observations prove that there is a direct connection between heating rate, causing melting and the structure obtained after subsequent solidification during cooling, as previously reported in the case of solid state transitions such as martensitic transformation [19].

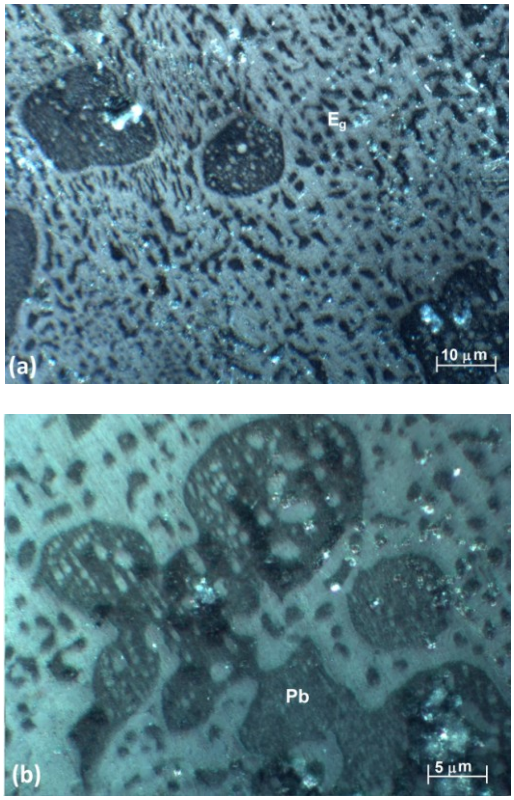

Fig. 9. OM micrograph of the specimen heated with 10K/min: (a) general aspect, with globular eutectic (E_g); (b) f Pb-rich areas

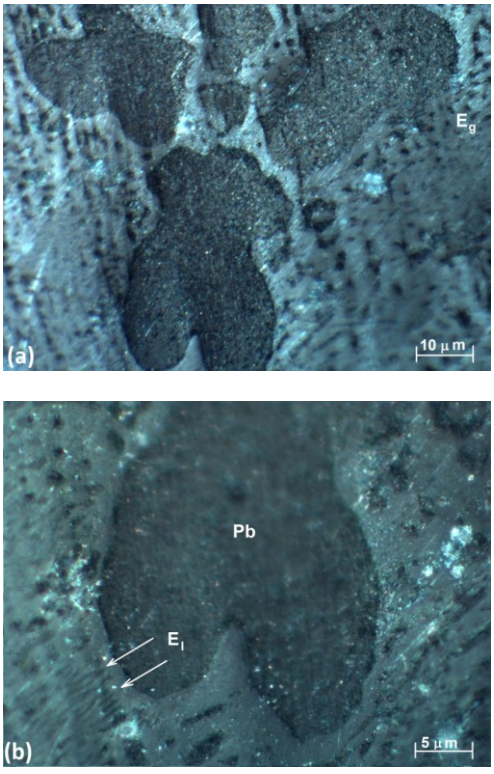

Fig. 10. OM micrograph of the specimen heated with 20K/min: (a) general aspect, with globular eutectic (E_g) areas; (b) large Pb-rich constituent and traces of lamellar eutectic (E_l) areas

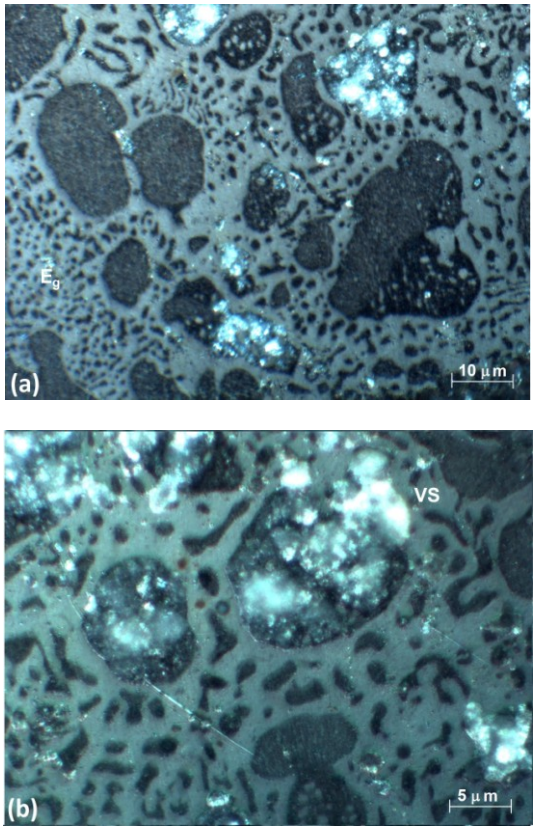

Fig. 11. OM micrograph of the specimen heated with 40K/min: (a) general aspect, with globular eutectic (E_g); (b) detail of the superposition of vitrified sand (VS) over pro-eutectic Pb

5. Summary and conclusions

The law of variation of the dissolution depth, caused by the M-effect, allows developing a mathematical model able to determine the operation times of HBC fuses under various overloads, from the minimum one required for melting till the maximum performance of the M-effect, jointly with the prediction of the ageing caused by recurrent overloads, permanent or not. Using the proposed solutions for the penetration depth of the eutectic alloy, only requires to know the process characteristics which can be obtained from simple experimental tests. Some values, *i.e.* the fuse diffusion coefficients, can be given by the manufacturer in datasheets, so that the user can get it and make simple calculation of fuse operating time in different overload conditions.

The structural effects of increasing electrical overloads on the melting of active eutectic parts of HBC fuses consisted in an increasing tendency of all critical temperatures of melting, associated with a morphological changing tendency, from lamellar to globular, of eutectic constituent.

Acknowledgements

This work was supported by UEFISCDI within the project PN-II-ID-PCE-2012-4-0033, contract no. 13/ 2013.

References

[1] A. Wright, P.G. Newbery, Electric Fuses, 3rd Ed., (IEE Power and Energy Series), p. 172 (2004).
[2] G. Chiriac, Electric Power Systems Research, **92**, 73 (2012).
[3] D. Rochette., R. Touzani, W. Bussiere, J Phys. D: Appl. Phys. **40**, 4544 (2007).
[4] M.A. Saqib, A.D. Stokes, IEEE Transactions on Power Delivery, **25** (1), 212 (2010).
[5] W. Bussiere, D. Rochette, G. Velleaud, T. Latchimy, J. L. Gelet, F. Gentils, J. C. Perez-Quesada, T. Rambaud and P. Andre, J Phys. D: Appl. Phys. **41**, 195210 (2008).
[6] S. Memiaghe, W. Bussiere, D. Rochette, R. Touzani, P. Andre, J of High Temp. Material Processes, **14** (3), 255 (2010).
[7] D.A. Beaujean, P.G. Newbery, M.G. Jayne, IEE Proc-A, **140** (4), 331 (1993).
[8] D.A. Beaujean, M.G. Jayne, P.G. Newbery, IEE Proc.-Sci. Meas. Technol., **142** (2), 162 (1995).
[9] M. Lindmayer, Proc. of the 6th Int. Conf. on Electric Fuses and their Applications, Torino, 13 (1999).
[10] A. Fogorosi, F. Blaabjerg, Industry Applications Conf., 39th IAS Annual Meeting, Conference, **4**, 2337 (2004).
[11] H.F. Farahani, M. Sabaghi, Indian J of Sci. and Technology, **5** (3), 2396 (2012).
[12] D.S. Petrovic, J. Medved, G. Klancnik, Materials and Technology, **47** (6), 831 (2013).
[13] K. Matsugi, G. Sasaki, O. Yanagisawa, Y. Kumagai, K. Fujii, Materials Transactions, **47** (9), 2413 (2006).
[14] K. Matsugi, H. Matsumoto, Y.B. Choi, G. Sasaki, K.I. Suetsugu, K.Fujii, Materials Transactions, **55** (3), 577 (2014).
[15] A. Etschmaier, G. Mori, W. Wegscheider, H. Wieser, Mat.-wiss. u. Werkstofftech. **33**, 90 (2002).
[16] B. Kosec, M. Sokoviæ, L. Kosec, M. Bizjak, F. Pusavec, Z. Kampus, Archives of Mater. Sci. and Engineering, **28** (4), 211 (2007).
[17] N. M. Lohan, B. Pricop, L.-G. Bujoreanu, N. Cimpoesu, Int. J. Mater. Res., **102** (11), 1345 (2011).
[18] R.F. Mehl, Metals handbook, 8th Edition, **7**, Atlas of Microstrutures of Industrial Alloys, ASM, Ohio, p. 297 (1972).
[19] N.M.Lohan, L.G.Bujoreanu, C.Baciu, Micro & Nano Letters, **7** (6), 540 (2012).

*Corresponding author: aplesca@tuiasi.ro